Journal of the Optical Society of Korea, Vol. 6, No. 3, September 2002, pp. 87-95

FDTD Simulation of Photonic-Crystal Lasers and Their Relaxation Oscillation

G. Hugh Song*, Soan Kim, and Kyuhwan Hwang

Department of Information and Communications, Kwangju Institute Science and Technology, Gwangju 500-712, KOREA

(Received August 12, 2002)

We have developed an finite-difference time-domain program that can analyze photonic devices with gain and/or dispersion. As an example, a two-dimensional photonic-crystal laser is simulated. The simulation can show the relaxation oscillation behavior at extremely high current injection.

OCIS codes : 130.0250, 130.3120, 140.3420, 270.2500.

I. INTRODUCTION

Recently, application of the finite-difference time-domain (FDTD) analysis [14] to various engineering problems is becoming practical owing to remarkable development of high-speed computers. The need for such a program in the analysis of photonic-crystal devices is especially recognized in that the capability of other conventional techniques such as the beam-propagation analysis and various types of frequency-domain analysis is seriously limited for the purpose.

Among many photonic-crystal devices, photonic-crystal lasers [1] attracted a considerable attention because the capability of such devices is not yet fully investigated since they have not been made close to perfection. Unlike conventional semiconductor lasers including vertical-cavity lasers, distributed-feedback (DFB) lasers, and distributed-Bragg-reflection (DBR) lasers, analysis of photonic-crystal lasers is relatively difficult because of their inherent fully-three-dimensional characteristics and their quite complicated modal and polarization characteristics. A considerable amount of research [5,13] is being carried on two-dimensional photonic-crystal lasers formed on a slab-waveguide of half-wavelength width. Design of the structure is made mostly with the operating principle of DBR in mind.

In this paper, we report on the development of a FDTD simulator which can analyze such photonic-crystal lasers. The gain medium is modeled by a region of an inverted carrier-density with the generalized Lorentz-dispersion characteristics, the idea of which appeared in [4] as a two-dimensional implementation for the application to a semiconductor amplifier structure. In this paper, we have gone further by doing a three-dimensional analysis to analyze a semiconductor laser structure with the interaction between the carriers and the electromagnetic fields fully integrated.

The regions for dispersive media and perfectly-matched layers (PML's) [2] are fully integrated in the code for full parallelization and efficient memory handling. For such a purpose, artificial layers of anisotropically dispersive electric/magnetic media [9] are introduced in all computation boundaries, while the recursive-convolution method [6] with the piecewise-constant approximation [11] has been used for simulation of both the dispersive media and the PML layers. We have found that this combination, which is being reported here for the first time, allows the most efficient coding and memory usage amenable to parallelization.

Both a fully three-dimensional version as well as the two-dimensional version of the simulator are developed simultaneously with almost all components of the code shared between the two versions. However, a three-dimensional simulation is necessary because in most cases of photonic-crystal lasers, we are certainly interested in the wave which radiates in the vertical direction after all. It is of unknown possibility that a clever two-dimensional simulation may well give a good amount of useful information in the case of semiconductor lasers of the edge-emitting type. However, we believe that a three-dimensional analysis is a must for the sake of confidence in most applications to simulations of photonic-crystal lasers of any material type.

As mentioned, analysis of the relaxation oscillation

of emitted optical power of the laser requires a feedback mechanism between the optical energy and the carriers in the active layer of the semiconductor. Here, a new kind of the rate equation for the number of electron carriers in the active layer has been developed for this purpose and solved numerically.

A great deal of the components of the simulator must work together to simulate the turn-on of the semiconductor photonic-crystal laser with a simulated gain spectrum with a characteristic relaxation oscillation behavior which have turned out to be rather unlikely in reality in such a small-size cavity semiconductor laser.

II. THE FINITE-DIFFERENCE TIME-DOMAIN METHOD WITH DISPERSION

We simulate the four Maxwell equations

$$\nabla \cdot \hat{\varepsilon}(\mathbf{r},\omega)\mathbf{E} = 0, \tag{1}$$

$$\nabla \cdot \hat{\mu}(\mathbf{r},\omega)\mathbf{H} = 0, \tag{2}$$

$$\nabla \times \mathbf{E} = \mathrm{i}\omega\hat{\mu}(\mathbf{r},\omega)\mathbf{H}, \tag{3}$$

$$\nabla \times \mathbf{H} = -\mathrm{i}\omega\hat{\varepsilon}(\mathbf{r},\omega)\mathbf{E}, \tag{4}$$

with the generalized electric permittivity tensor $\hat{\varepsilon}(\mathbf{r},\omega)$ and the magnetic permeability tensor $\hat{\mu}(\mathbf{r},\omega)$ with a certain type of frequency dependence. The two material tensors are "generalized" in the sense that

$$\frac{\partial\hat{\mathcal{D}}(\mathbf{r},t)}{\partial t} \equiv \int_{-\infty}^{\infty}[\mathbf{J}(\mathbf{r},\omega) - \mathrm{i}\omega\mathbf{D}(\mathbf{r},\omega)]\,\mathrm{e}^{-\mathrm{i}\omega t}\frac{\mathrm{d}\omega}{2\pi} \equiv -\int_{-\infty}^{\infty}\mathrm{i}\omega\hat{\varepsilon}(\omega)\mathbf{E}(\mathbf{r},\omega)\mathrm{e}^{-\mathrm{i}\omega t}\frac{\mathrm{d}\omega}{2\pi}. \tag{5}$$

where $\mathbf{J}(\mathbf{r},\omega)$ refers to the current density due to motion of free carriers

1. Perfectly-matched layers

In the PML, according to the algorithm of perfectly-matched anisotropic layers [9], the electric permittivity and the magnetic permeability are expressed as

$$\hat{\varepsilon}(\mathbf{r},\omega) \equiv \hat{\varepsilon}(\omega)\mathbf{\Lambda}(\mathbf{r},\omega), \tag{6}$$

$$\hat{\mu}(\mathbf{r},\omega) \equiv \begin{cases} \mu_0\mathbf{\Lambda}(\mathbf{r},\omega), & \text{in the PML,} \\ \mu_0, & \text{in the inner dispersive region,} \end{cases} \tag{7}$$

where $\hat{\varepsilon}(\omega)$ is the electric permittivity of the inner region, while the tensor of a diagonal matrix $\mathbf{\Lambda}(\mathbf{r},\omega)$ is shared in the PML as a factor between the electric permittivity and the magnetic permeability. The lth diagonal element can be expressed as

$$\Lambda_{ll}(\mathbf{r},\omega) \equiv 1 + \sum_{p=1}^{M_l}\frac{\Gamma_l^{(p)}(\mathbf{r})}{-\mathrm{i}\omega - s_l^{(p)}} + \frac{Q_l(\mathbf{r})}{-\omega^2} \quad l = \mathrm{x},\mathrm{y},\mathrm{z}, \tag{8}$$

where M_l is the order of the rational function representing the lth diagonal component of the permittivity in the region containing the position denoted by $\mathbf{r}$.

2. Gain dispersive medium

In the inner region of dispersion, the three diagonal elements are basically the same, which represents an isotropic material of dispersion with gain or loss. In order for the dipole resonance to be expressed mathematically as a real function of time, all the poles, other than the ones on the imaginary axis of the complex-ω plane, and their corresponding residues should exist in complex-conjugate pairs, so that the simplest implementation of the gain medium is modeled as the electric-permittivity function of

$$\hat{\varepsilon}(\omega) \equiv \hat{\varepsilon}(\infty)\left\{1 + \sum_{q=1}^{N}\left[\frac{\Gamma^{(q)}}{-\mathrm{i}\omega - s^{(q)}} + \frac{\Gamma^{(q)*}}{-\mathrm{i}\omega - s^{(q)*}}\right]\right\}. \tag{9}$$

We should choose $\hat{\varepsilon}(\infty)$ as the base electric permittivity by which the background spectrum of the electric permittivity of the medium, representing the contribution from the dipole resonance at frequencies substantially higher than the spectral range of interest, is adequately taken care of. It should thus be different from the true physical permittivity at $\omega \to \infty$. N is the number of pole pairs, each of which forms a so-called Lorentzian function unit in the form of

$$\chi^{(q)}(\omega) \equiv \frac{N_\mathrm{e}\,q_\mathrm{e}^2}{m_\mathrm{e}\varepsilon_0}\frac{f_q}{2\omega_q}\left[\frac{1}{\omega - \omega_q + \mathrm{i}\gamma_q} - \frac{1}{\omega + \omega_q + \mathrm{i}\gamma_q}\right] \simeq \frac{N_\mathrm{e}\,q_\mathrm{e}^2}{m_\mathrm{e}\varepsilon_0}\frac{f_q}{\omega_q^2 - \omega^2 - \mathrm{i}2\gamma_q\omega}, \tag{10}$$

participating for the total sum in the right-hand side of (9).

The poles and residues are matched to the resonance frequencies ω_q and the damping constants γ_q as

$$s^{(q)} \equiv -\gamma_q + \mathrm{i}\omega_q, \tag{11}$$

$$\Gamma^{(q)} \equiv \frac{\hat{\varepsilon}(0) - \hat{\varepsilon}(\infty)}{\varepsilon_0}\frac{f_q\omega_q}{\mathrm{i}2}, \tag{12}$$

where f_q is the oscillator strength of the qth resonance, satisfying the sum rule;

$$\sum_{q=1}^{N} f_q = 1. \tag{13}$$

Physically, dispersion accompanies either gain or loss. It is well-known that a status of so-called population inversion is required for the material to provide gain for a passing optical wave. The population inversion is represented the most properly by a negative parameter for the available number of dipoles N_e. In simulation, it is parameterized by a negative number for $\hat{\varepsilon}(0) - \hat{\varepsilon}(\infty)$.

3. The recursive-convolution technique with the anisotropic PML

The key to the FDTD simulation on a dispersive medium is in the implementation of (5) in the time domain. We express each vector component as

$$\hat{\mathcal{D}}_l(\mathbf{r},t) = \int_{-\infty}^{t} \check{\varepsilon}_{ll}(t-t')\mathcal{E}_l(\mathbf{r},t')\,dt', \tag{14}$$

i.e., a convolution of $\mathcal{E}_l(\mathbf{r},t)$ with each element of the inverse Fourier transform of the diagonal tensor $\hat{\varepsilon}(\mathbf{r},\omega)$ of (6), expressed as

$$\begin{aligned}\check{\varepsilon}_{ll}(\mathbf{r},t) &\equiv \int_{-\infty}^{\infty} \hat{\varepsilon}(\omega)\Lambda_{ll}(\mathbf{r},\omega)\mathrm{e}^{-\mathrm{i}\omega t}\frac{\mathrm{d}\omega}{2\pi} \\ &\equiv \hat{\varepsilon}(\infty)\left[\delta(t) + \sum_{q=1}^{N_l} \mathrm{Re}\check{\chi}_l^{(q)}(\mathbf{r},t) + Q_l\, t\, \theta(t)\right] \end{aligned} \tag{15}$$

with

$$\check{\chi}_l^{(q)}(\mathbf{r},t) \equiv R_l^{(q)}(\mathbf{r})\theta(t)\exp\left(s_l^{(q)}t\right), \tag{16}$$

where $\delta(t)$ is the Dirac delta function, and $\theta(t)$ is the Heaviside step function defined to be 1 for $t > 0$ or 0, otherwise. Subscript l has been appended to N of (9) for (15), counting the "reduced" number of simple poles of the rational function correctly, for the purpose of combining the case of Lorentzian dispersion and that of the PML. For the two symmetrically paired poles of each Lorentzian spectral function in each term of the summation in (9), only one pole is counted in with an appropriate modification of its corresponding residue for $\check{\chi}_l^{(q)}(t)$ in (16) as

$$R_l^{(q)} = 2\Gamma^{(p)}, \tag{17}$$

which is pure-imaginary, according to (12). Thus, this procedure allows simplification in the case of paired Lorentzian poles in line with the case of simple poles. That is, for all other terms, $R_l^{(q)} = \Gamma_l^{(p)}$ and is real.

We have employed the piecewise-constant recursive-convolution technique which was first introduced in Ref. [11]. Accordingly, fields, e.g., $\mathcal{E}_x(\mathbf{r},t)$, are approximated numerically as

$$\mathcal{E}_l(\mathbf{r},t) \simeq \mathcal{E}_l|^n \tag{18}$$

for $[n-1/2]\,\Delta t < t < [n+1/2]\,\Delta t$, where Δt is the width of each time step in the FDTD simulation. The advantage of using this scheme over the piecewise-linear approximation scheme, which was introduced actually more recently in Ref. [3] than the piecewise-constant scheme in Ref. [11], resides in the fact that the latter needs the field values in just the previous time step unlike the former requiring those in two time steps. It is thus considered as probably the best compromise between the speed and accuracy of the result of the FDTD simulation for dispersive media.

Based on the piecewise-constant approximation scheme, formulas suitable for numerical implementation are rederived as

$$\left[\frac{1}{\Delta t} + \sum_{q=1}^{N_l} \mathrm{Re}\check{\chi}_l^{(q)}|^{0,1/2}\right]\mathcal{E}_l|^{n+1} \tag{19}$$

$$\begin{aligned} &= \left[\frac{1}{\Delta t} - \sum_{q=1}^{N_l} \mathrm{Re}\check{\chi}_l^{(q)}|^{-1/2,0}\right]\mathcal{E}_l|^n \\ &\quad - \sum_{q=1}^{N_l} \mathrm{Re}\left\{\left[1-\mathrm{e}^{-s_l^{(q)}\Delta t}\right]\Phi_{\mathcal{E}_l}^{(q)}|^{n+1}\right\} - Q_l\mathcal{I}_{\mathcal{E}_l}|^{n+1/2} \\ &\quad + \frac{\hat{\mathbf{r}}_l\cdot\nabla\times\mathcal{H}|^{n+1/2}}{\hat{\varepsilon}(\infty)}, \end{aligned} \tag{20}$$

where $\hat{\mathbf{r}}_l\cdot\nabla\times\mathcal{H}$ represents the lth component of the vector obtained by the curl operation in the spatial-difference form. The above relation along with recursive relations for $\Phi_{\mathcal{E}_l}^{(q)}|^n$ and $\mathcal{I}_{\mathcal{E}_l}|^n$ given as

$$\Phi_{\mathcal{E}_l}^{(q)}|^{n+1} = \left\{\left[\check{\chi}_l^{(q)}|^{0,1/2} + \check{\chi}_l^{(q)}|^{-1/2,0}\right]\mathcal{E}_l|^n + \Phi_{\mathcal{E}_l}^{(q)}|^n\right\} \times \mathrm{e}^{s_l^{(q)}\Delta t}, \tag{21}$$

$$\mathcal{I}_{\mathcal{E}_l}|^{n+1/2} = \mathcal{I}_{\mathcal{E}_l}|^{n-1/2} + \mathcal{E}_l|^n, \tag{22}$$

Note that (20)–(21) are written in terms of $\check{\chi}_l^{(q)}|^{0,1/2}$ and $\check{\chi}_l^{(q)}|^{-1/2,0}$ only. Unlike the simple approximation in (18) or the two other mentioned schemes for field values, these two parameters are to be evaluated at a level of much higher accuracy, by an appropriate integral over the exponential shape of the $\chi_l^{(q)}(t)$ function. That is,

$$\check{\chi}_l^{(q)}|^{n,n'} \equiv \frac{1}{\Delta t}\int_{n\Delta t}^{n'\Delta t} \check{\chi}_l^{(q)}(t)\,dt \tag{23}$$

yielding the following results;

$$\check{\chi}_l^{(q)}|^{0,1/2} = R_l^{(q)}\mathrm{exprl}(s_l^{(q)}\Delta t/2), \tag{24}$$

$$\check{\chi}_l^{(q)}|^{-1/2,0} = R_l^{(q)}\,\mathrm{exprl}(-s_l^{(q)}\Delta t/2) \tag{25}$$

with

$$\mathrm{exprl}z \equiv \begin{cases} 1, & z = 0, \\ \dfrac{\exp z - 1}{z}, & \text{otherwise.} \end{cases} \tag{26}$$

Eq. (20) thus provides the needed algorithm which allows systematic treatment for the dispersive material in FDTD simulations with the least amount of computer memory for the iterative time-stepping computation.

An almost identical form of the difference equation gives an expression for the update of the magnetic field because the electric susceptibility and the magnetic susceptibility share exactly the same tensor structure in the PML, as indicated in (6)–(7), and $\mu = \mu_0$ in the inner regions. Hence, in the PML,

$$\left[\frac{1}{\Delta t} + \sum_{q=1}^{N_l} \mathrm{Re}\check{\chi}_l^{(q)}|^{0,1/2}\right] \mathcal{H}_l|^{n+1/2} = \left[\frac{1}{\Delta t} - \sum_{q=1}^{N_l} \mathrm{Re}\check{\chi}_l^{(q)}|^{-1/2,0}\right] \mathcal{H}_l|^{n-1/2} - \sum_{q=1}^{N_l} \mathrm{Re}\left\{\left[1 - \mathrm{e}^{-s_l^{(q)}\Delta t}\right] \Phi_{\mathcal{H}_l}^{(q)}|^{n+1/2}\right\} - Q_l \mathcal{I}_{\mathcal{H}_l}|^n + \frac{\hat{\mathbf{r}}_l \cdot \nabla \times \mathcal{E}|^n}{\mu_0} \quad (27)$$

with

$$\Phi_{\mathcal{H}_l}^{(q)}|^{n+1/2} = \left\{\left[\check{\chi}_l^{(q)}|^{0,1/2} + \check{\chi}_l^{(q)}|^{-1/2,0}\right] \mathcal{H}_l|^{n-1/2} + \Phi_{\mathcal{H}_l}^{(q)}|^{n-1/2}\right\} \exp(s_l^{(q)}\Delta t) \quad (28)$$

again in terms of $\check{\chi}_l^{(q)}|^{0,1/2}$ and $\check{\chi}_l^{(q)}|^{-1/2,0}$ only. The contribution from double poles is computed by another recurrence relation

$$\mathcal{I}_{\mathcal{H}_l}|^n \equiv \mathcal{I}_{\mathcal{H}_l}|^{n-1} + \mathcal{H}_l|^n. \quad (29)$$

In the inner region with $\mu = \mu_0$, a much simpler equation as

$$\frac{\mathcal{H}_l|^{n+1/2}}{\Delta t} = \frac{\mathcal{H}_l|^{n-1/2}}{\Delta t} + \frac{\hat{\mathbf{r}}_l \cdot \nabla \times \mathcal{E}|^n}{\mu_0} \quad (30)$$

suffices.

III. MODEL FOR THE GAIN MEDIUM AND THE POPULATION INVERSION

The gain-dispersion characteristics of the active semiconductor medium are modeled by the Lorentzian formula of Eq. (9) with a single pair of poles. Evidently, it is a rather gross simplification for the inhomogeneously broadened gain-spectrum structure of any semiconductor medium. For the simulation of the gain medium, we performed an "experimental" fit between location of the poles and the carrier density of in the active region to obtain its relation to the numbers for γ_1 and ω_1. Therefore,

$$s^{(1)} \equiv -\gamma_1 + \mathrm{i}\omega_1, \quad (31)$$

Having a model with the dispersion and gain will result in a perturbation in the refractive index. Relatively speaking, this perturbation does not appear critically important because the $\hat{\varepsilon}(\infty)/\varepsilon_0$ is present in the background. However, the perturbation in the imaginary part is crucial. The peak gain happens at $\omega = \omega_1$. Out of the two terms with the minus sign in front,

$$\mathrm{Im}\chi(\omega_1) \equiv -2\,\frac{\omega_1}{c}\sqrt{\frac{\hat{\varepsilon}(\omega_1)}{\varepsilon_0}} \simeq \frac{\hat{\varepsilon}(0) - \hat{\varepsilon}(\infty)}{\varepsilon_0}\frac{\omega_1}{2\gamma_1}\left[p^{\mathrm{I}} - p^{\mathrm{II}}\right] \quad (32)$$

must be related to

$$\mathcal{G}(\omega_1) \simeq -\frac{\omega_1}{c}\frac{\mathrm{Im}\hat{\varepsilon}}{\sqrt{\varepsilon_0 \mathrm{Re}\hat{\varepsilon}}} \simeq -\frac{\omega_1}{c}\frac{\mathrm{Im}\hat{\chi}}{n'} = \frac{\omega_1^2}{2n'c\gamma_1}\frac{\hat{\varepsilon}(0) - \hat{\varepsilon}(\infty)}{\varepsilon_0}\left[p^{\mathrm{II}} - p^{\mathrm{I}}\right], \quad (33)$$

where n' is the real refractive index of the medium. The factor $p^{\mathrm{II}} - p^{\mathrm{I}}$ in both relations can be replaced by $2p^{\mathrm{II}} - 1$. However, the individual probabilities should find themselves in the expressions for the respective residues from the known parameter values of γ_1 and $\hat{\varepsilon}(0) - \hat{\varepsilon}(\infty)$.

IV. INTERACTION BETWEEN LIGHT AND MATTER

Beside the amplification of the propagating light which is present in the medium, there exists spontaneous emission which actually provides the seed for the amplifying light in the medium. Such emission of light is modeled by a randomly oriented polarization current density with the magnitude properly determined in each cell of the FDTD model.

When the active layer of the semiconductor is overly populated by the established difference ΔE_{F} between the two quasi-Fermi levels, the spontaneous emission is enhanced according to

$$\frac{\mathrm{d}}{\mathrm{d}t}\langle n_\kappa(t)\rangle = G_\kappa\left[\langle n_\kappa(t)\rangle - n_\kappa^{\mathrm{sp}}\right] - \frac{\langle n_\kappa(t)\rangle - n_\kappa^{\mathrm{eq}}}{\tau_\kappa^{\mathrm{ph}}}, \quad (34)$$

where

$$-G_\kappa n_\kappa^{\mathrm{sp}} \equiv \frac{1}{\exp([\hbar\omega_\kappa - \Delta E^{\mathrm{F}}]/k_{\mathrm{B}}T) - 1} \quad (35)$$

accounts for the rate of spontaneous emission enhanced from that of thermal equilibrium owing to pumping causing $\Delta E^{\mathrm{F}} > 0$. These two sources of light generation can be implemented in the FDTD simulator, once each module is properly prepared.

The additional polarization field in the presumed absence of the dipoles resonating at the lasing frequency is included in $\hat{\varepsilon}(\infty)\mathcal{E}(\mathbf{r},t)$ presumably with no dispersion. The additional polarization field in the presumed absense of the dipoles resonating at the lasing frequency is included in $\hat{\varepsilon}(\infty)\mathcal{E}(\mathbf{r},t)$. In actual simulation, one can only put the permittivity value sufficiently beyond the lasing frequency and, if optical pumping is being simulated as well, the pump frequency. We have denoted this permitivity value by $\hat{\varepsilon}(\infty)$ in

$$\hat{\mathcal{D}}(\mathbf{r},t) \equiv \hat{\varepsilon}(\infty)\mathcal{E}(\mathbf{r},t) + \hat{\mathcal{P}}^{\mathrm{l}}(\mathbf{r},t) + \hat{\mathcal{P}}^{\mathrm{p}}(\mathbf{r},t), \qquad (36)$$

where $\hat{\mathcal{P}}^{\mathrm{l}}(\mathbf{r},t)$ and $\hat{\mathcal{P}}^{\mathrm{p}}(\mathbf{r},t)$ represent the polarization fields due to interaction (mostly emission) of light at the lasing frequency and due to interaction (mostly absorption) at pump frequency, respectively.

Similar to a case of the dynamic simulation [7] based on the analysis of resonance modes on a semiconductor laser, we need a rate equation which updates the number of carriers inside the active region. The equation can be obtained by considering the classical theorem of J. H. Poynting in regard to the energy balance [12]. According to the theorem,

$$\nabla\cdot\mathcal{E}^{\mathrm{l}}\times\mathcal{H}^{\mathrm{l}} + \frac{\mu_0}{2}\frac{\partial}{\partial t}\mathcal{H}^{\mathrm{l}}\cdot\mathcal{H}^{\mathrm{l}} + \frac{\hat{\varepsilon}(\infty)}{2}\frac{\partial}{\partial t}\mathcal{E}^{\mathrm{l}}\cdot\mathcal{E}^{\mathrm{l}} + \mathcal{E}^{\mathrm{l}}\cdot\frac{\partial\hat{\mathcal{P}}^{\mathrm{l}}}{\partial t} = 0. \qquad (37)$$

The polarization current $\partial\mathcal{P}^{\mathrm{l}}/\partial t$ in the last term of the left-hand side represents the interaction of the external field and the dipoles in the semiconductor active medium. This term is balanced with the energy which is provided either by the injection current or by the pumping light.

For the case of current injection, the rate equation can be written as

$$\iiint_{V_{\mathrm{q}}} \mathcal{E}^{\mathrm{l}}\cdot\frac{\partial\hat{\mathcal{P}}^{\mathrm{l}}(\mathbf{r},t)}{\partial t}\,d^3\mathbf{r} - \hbar\omega_{\mathrm{l}}\left[\frac{\mathrm{d}N_{\mathrm{e}}(t)}{\mathrm{d}t} - \frac{I^{\mathrm{qs}}(t)}{q_{\mathrm{e}}}\right] = 0, \qquad (38)$$

where

$$N_{\mathrm{e}}(t) \equiv \iiint_{V_{\mathrm{q}}} n_{\mathrm{e}}(\mathbf{r},t)\,d^3\mathbf{r} \qquad (39)$$

is the total number of carriers in the active layer of volume V_{q}, and $I^{\mathrm{qs}}(t)$ is the injection current. Here, $\hbar\omega_{\mathrm{l}}$ is the energy of a single photon at lasing frequency.

It has been assumed that some minor optical processes such as free-carrier absorption and various optical scattering processes are ignored.

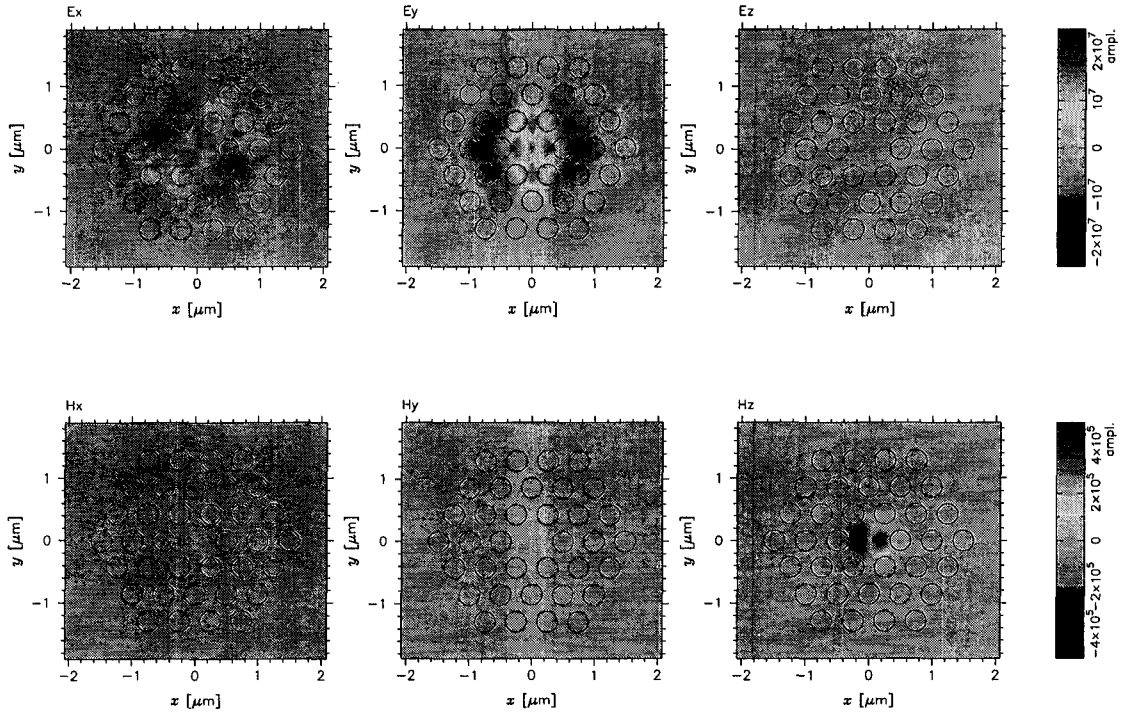

FIG. 1. Simulated field profile of the lasing mode built-up in a photonic crystal microcavity. The three plots in the right column show the snapshots of $\mathcal{E}_{\mathrm{x}}$, $\mathcal{E}_{\mathrm{y}}$, and $\mathcal{E}_{\mathrm{z}}$, while those of the left column show the snapshots of $\mathcal{H}_{\mathrm{x}}$, $\mathcal{H}_{\mathrm{y}}$, and $\mathcal{H}_{\mathrm{z}}$.

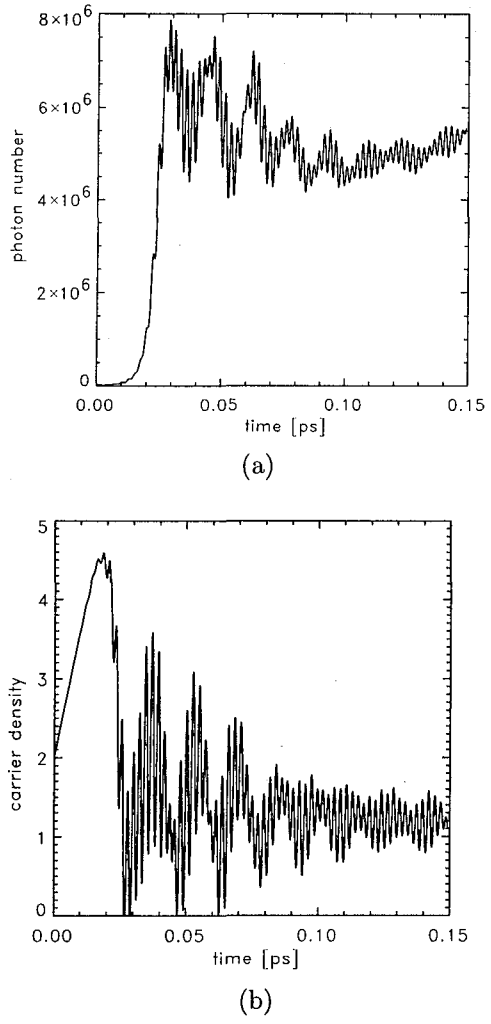

FIG. 2. The relaxation oscillation behavior obtained from the three-dimensional simulator at the simulated current level of 30 A. (a) The photon numbers in the microcavity (b) the average carrier density.

V. THREE-DIMENSIONAL SIMULATION RESULTS

From the considerations in the foregoing sections, we have performed a three-dimensional calculation on a structure which has become well-known from the publication of its structure once published in Science [8]. In the simulation, we assumed the case of current injection instead of optical pumping in their experiment. As mentioned previously, the choice of the two-dimensional simulator and the method of pumping is largely driven by the need in the development stage of the simulator which requires a tremendous amount of computer resources in terms of computing time and memory. We first tried to find the condition for the relaxation oscillation while we are finding the lasing optical mode. As expected from the known property [10] of the triangular lattice structure with a single defect made of a missing hole at the center, the lasing mode has been found to be the doubly-degenerate dipole-shaped field as shown in Fig. 1. The animation obtained from the simulator has shown that the axis of the dipole field is constantly rotating. It confirms that the mode is doubly-degenerate as the theory indicates.

The two plots of Fig. 2 show the familiar appearances at a certain level of current injection. The magnitude of the injected current has been set at 30 amperes which is unrealistically high. This choice has been made to show the relaxation oscillation which has been regarded as one of the lasing properties of a typical semiconductor laser.

To understand why such a high injection current is required to observe the relaxation oscillation, we made

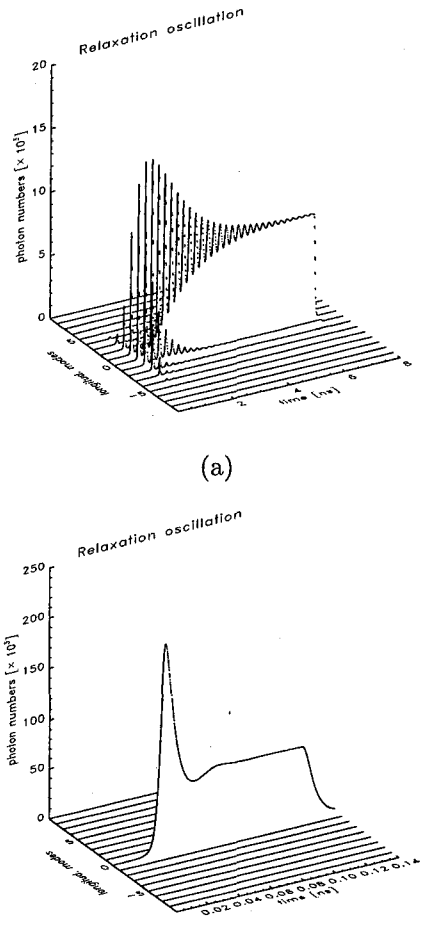

FIG. 3. Excitation of several longitudinal modes showing relaxation oscillation behavior. (a) In a semiconductor laser of a typical size driven by current level of 10 mA. (b) In a microcavity laser with the mode volume of 5 μm^3) driven by a 100 mA.

a small well-known mode based simulation on the evolution of longitudinal modes. However, as shown in Fig. 3, only excessive high injection current makes the oscillation speed sufficiently high for any relaxation oscillation to show up. This can be explained by carefully considering the sign of

$$\left[\frac{\gamma_\kappa - \gamma_N}{2}\right]^2 + \mathcal{K}_{\mathrm{p}N}\mathcal{K}_{N\mathrm{p}} \tag{40}$$

from the analytic formula for relaxation oscillation. Here, γ_N and γ_κ are the damping constants for the carrier density fluctuation and for the photon density fluctuation, respectively, and $\mathcal{K}_{N\kappa}$ and $\mathcal{K}_{\kappa N}$ are the two coupling coefficients between the two small-signal rate equations for the carrier density and the photon density, respectively.

For a micro-cavity laser, the value of the $\mathcal{K}_{N\kappa}\mathcal{K}_{\kappa N}$ becomes a relatively small negative number. In order to observe any relaxation oscillation, we should drive up the injection current unrealistically high. That is the reason that our simulation has required an unrealistically high injection current. In a different perspective, we may state that the relaxation oscillation should not be considered as the characteristic properties of a semiconductor laser.

At the practical level of either optical pumping or current injection, we conclude that the microcavity laser of this kind will not show the relaxation oscillation behavior at the practical level of current injection.

1. Band-edge photonic-crystal lasers

If the photonic-crystal structure does not have the center defect, the structure can be considered a two-dimensional analog to the one-dimensional structure which is usually called the distributed feedback laser rather than a distributed Bragg reflection laser with the center quarter-wave phase mismatch in the middle.

The field profile of the lasing mode of such a band-edge photonic-crystal laser is given in Fig. 4.

The basic working principle of the so-called band-edge laser is the same as a conventional DFB laser in that a DFB laser as the one-dimensional analog oscillates at frequency of the two band edges of the stop band created by the periodic structure. In order to confirm such a behavior, we have simulated by aligning the peak of the gain spectrum at the top edge of lower band as shown in Fig. 5 The normalized resonance frequency from simulation has been found at $ka/2\pi = 0.32$ which agreed nicely with the normalized frequency at the top of the lowest photonic band at the K point in the two-dimensional reciprocal space.

The relaxation behavior of the carrier denstiy and the photon occupation number in the cavity is shown in Fig. 6. Unlike Fig. 2(a), there exists some initial anomaly in the relaxation curve for the photon occupation number. With the complexity of the distribu-

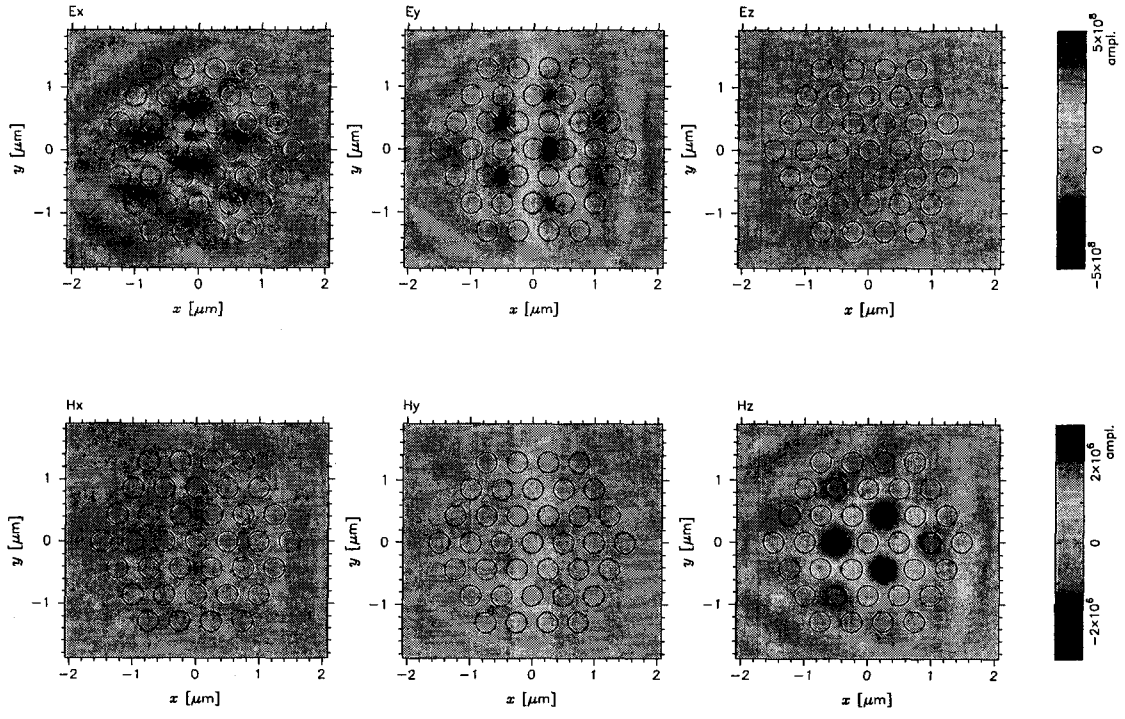

FIG. 4. Field profle of the band-edge photonic-crystal laser.

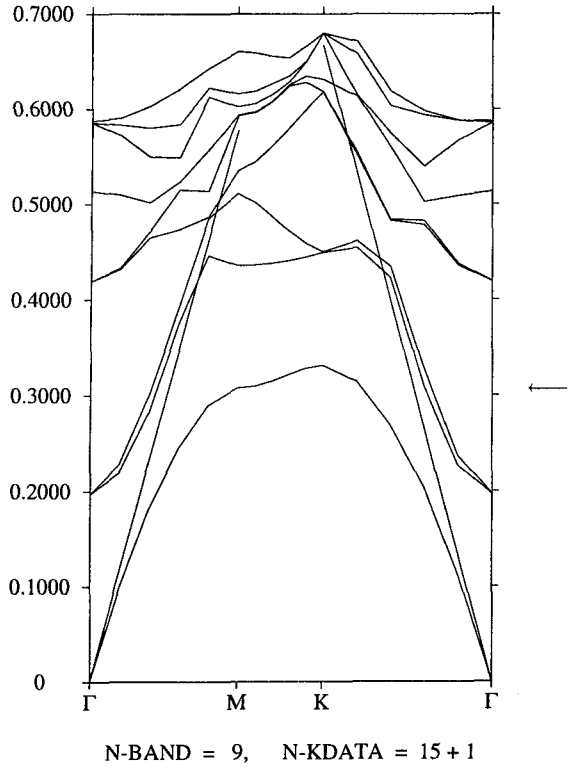

FIG. 5. Confrmation of the oscillation frequency in the band-edge photonic crystal laser. The arrow in the right indicates the frequency at the top of the first band ($ka/2\pi = 0.32$) obtained at the K point in the reciprocal space.

ted-gain medium of a DFB laser being considered, such an anomaly appears to be the result of the transient operating point seeking its steady state.

VI. SUMMARY

In summary, we have developed a three-dimensional FDTD simulator in which the scheme of anisotropic PML's and the piecewise-constant approximation for recursive-convolution integral are integrated for the numerical analysis of a gain medium with the Lorentzian dispersion spectrum. With this new functionality of the simulator, we have been able to numerically create a situation for relaxation oscillation. The preliminary result suggests that the lasers of this kind will not show the typical relaxation oscillation except the initial overshoot of the light output at the initial turn-on time-delay.

We then performed a simulation of a two-dimensional distributed-feedback photonic-crystal microcavity laser in which the imaginary part of the dispersion function of the medium plays an essential role in its choice of the lasing frequency and the noise characteristics. There are a number of findings from the

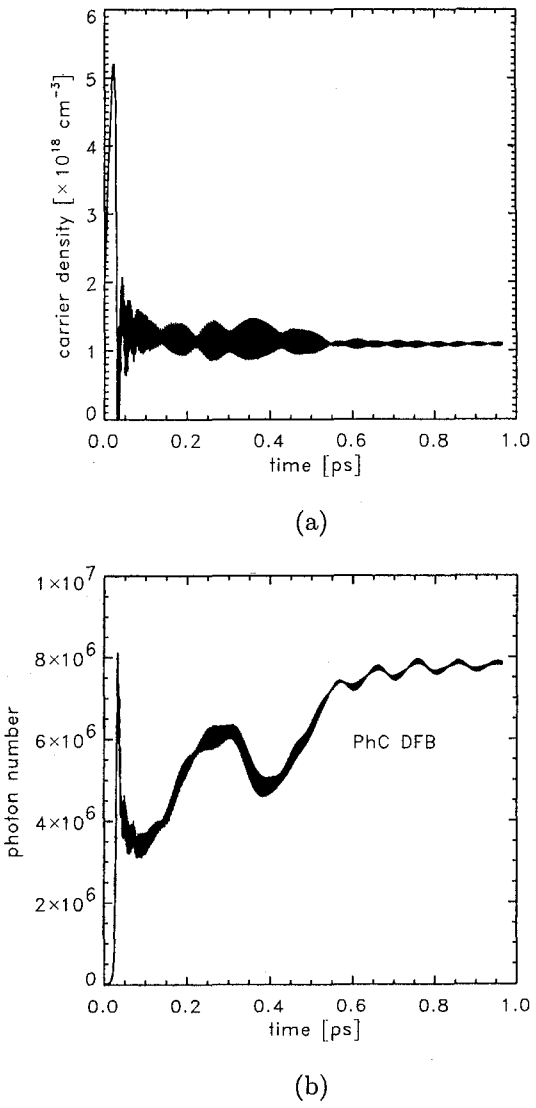

FIG. 6. Relaxation oscillation behavior of carrier density and the photon occupation number of a two-dimensional DFB laser.

simulation, each of which need to be carefully studied for its physical implication. These are the topics of future study.

ACKNOWLEDGMENTS

We thank Prof. Y. H. Lee of KAIST for a number of discussions in band-edge photonic-crystal lasers. This work has been supported in part by the Institute of Information Technology Assessment through the CHOAN Program, by the Korea Science and Engineering Foundation through the UFON ERC Program, and by the Ministry of Education through the

BK-21-IT Program.

*Corresponding author : ghsong@kjist.ac.kr.

REFERENCES

[1] T. Baba, IEEE J. Sel. Topics on Quantum Electron. **3**, 808 (1997).
[2] J. -P. Berenger, J. Computational Physics **114**, 185 (1994).
[3] G. -X. Fan and Q. H. Liu, IEEE Trans. Antennas Propagat. **48**, 634 (2000).
[4] R. J. Hawkins and J. S. Kallman, Optical and Quantum Electronics **26**, S207 (1994).
[5] J. K. Hwang, H. Y. Ryu, D. S. Song, I. Y. Han, H. K. Park, D. H. Jang, and Y. H. Lee, IEEE Photonics Technol. Lett. **12**, 1295 (2000).
[6] R. J. Luebbers and F. Hunsperger, IEEE Trans. Antennas Propagat. **21**, 1087 (1953).
[7] D. Marcuse and T. P. Lee, IEEE Quantum Electron. **QE-19**, 1397 (1983).
[8] O. Painter, R. K. Lee, A. Yariv, A. Scherer, J. D. O' Brien, P. D. Dapkus, and I. Kim, *Science* **284**, 1819 (1999).
[9] Z. S. Sacks, D. M. Kingsland, R. Lee, and J. -F. Lee, IEEE Trans. Antennas Propagat. **43**, 1460 (1995).
[10] K. Sakoda, *Optical Properties of Photonic Crystals* (Springer, Berlin, 2001).
[11] J. Schuster and R. J. Luebbers, IEEE Antennas and Propagation Soc. Internat. Symp. Digest 2018 (1998).
[12] G. H. Song, *Principles of Photonics* (Classnote, Kwangju Institute of Science and Technology, Not yet published, 2002).
[13] J. Vučković, O. Painter, Y. Xu, A. Yariv, and A. Scherer, IEEE J. Quantum Electron. **35**, 1168 (1997).
[14] K. S. Yee, IEEE Trans. Antennas Propagat. **14**, 302 (1966).